Airfoil Computation at High Angles of Attack, Inviscid and Viscous Phenomena

John T. Barton* and Thomas H. Pulliam†
NASA Ames Research Center, Moffett Field, California

An implicit central difference code is used to calculate two-dimensional inviscid and thin-layer Navier-Stokes solutions for flow about an NACA 0012 airfoil at high angles of attack. Among the issues addressed are whether separation can occur in an inviscid calculation and what the causes would be of such separation. Examples are shown of inviscid shocked flow with and without separation and shock-free flow with separation. An Euler solution with self-induced oscillation and separation driven by a strong shock is contrasted with a shock-free solution whose separation is caused by numerical error. Computed solutions to the Euler equations are compared to those of the potential equations. Comparisons are also made between experimental data from wind tunnel tests and viscous calculations at similar conditions.

Introduction

THE existence of flow separation and recirculation is usually associated with viscous flows. The physical basis is fairly well understood and has been extensively studied. There are a number of physical phenomena that cause flow separation and recirculation. In all cases in which recirculation is present, vorticity must also be present and, thus, there must exist some mechanism that generates vorticity. In a viscous wall-bounded flow, the boundary layer generates a velocity gradient, vorticity, and momentum losses. In the presence of an adverse pressure gradient, separation can occur with the subsequent development of a recirculating reverse flow region and possible reattachment. A shock impinging on a boundary layer can cause flow separation. The governing equations for these types of flows are the Navier-Stokes equations or some subset of them.

Recently, there has been considerable interest in the numerical solution of the inviscid flow equations (the Euler equations). For most of the work reported in the literature, the accuracy of the results is quite good and the solutions obtained are representative of the physical flow of interest. For instance, when viscous effects are negligible, such as for thin boundary layers, the inviscid solutions are a good approximation to the solution of the full Navier-Stokes equations. In this situation, certain quantities, such as the pressure along the body, can be predicted well by the Euler equations. In contrast, numerical solutions to the Euler equations have been reported that do not have a straightforward physical interpretation. In particular, flow separation and recirculation for solutions to the Euler equations have been reported by a number of researchers (e.g., Salas[1]). The question naturally arises as to the physical interpretation of these flows in the absence of physical viscosity. In trying to attach any physical meaning to these flows, we must first examine the possible mechanisms that could generate vorticity.

Actual fluid flow is never truly inviscid, although in some cases the viscous effects are negligible. In computations, however, we can solve numerical approximations to the Euler equations. The solution of the Euler equations is typically much faster and more robust than the Navier-Stokes equations. One of the main reasons for this lies not in the codes themselves, but in the highly refined grids that are required to resolve the boundary layers in viscous calculations. These meshes cause the resulting finite difference equations to be very stiff and stability limits arising from the associated large CFL numbers often mandate that the time step increments be very small. Therefore, it is more economical to use the Euler equations to solve a fluid flow problem. Consequently, it is of great value to know when the Euler equations will give an answer that is good enough, by which is meant the following: the computed quantities of interest are sufficiently similar to those arising from the Navier-Stokes equations.

As a corollary, it is also of value to know when a numerical solution to the Euler equations is still valid and accurate, even though it is not a good approximation to the Navier-Stokes equations. The solution of the Euler equations for airfoils at high angles of attack produces these types of flow. In this paper, we present computations with inviscid flow recirculation (reverse flow regions) that are claimed to be valid solutions of the Euler equations. The direct mechanism for these flows is the generation of vorticity and the proper convection of that vorticity, both of which are implied by the Euler equations and which can be accurately computed by a numerical procedure.

Although the Euler equations do not provide for vorticity creation due to shear stress (which requires viscosity), vorticity may arise at shocks in the flow. Curved shock waves near surfaces generate a velocity gradient due to the variation in strength along the shock. This is one mechanism for the introduction of vorticity in an inviscid flow. Strong shock waves will cause a large entropy production; and if a strong shock extends only over a short distance, there will be a gradient in the downstream velocity along the shock and, consequently, vorticity will be created and shed downstream.

It is well known that the conventional computational solutions to the Euler equations contain some sort of numerical boundary conditions and artificial viscosity (dissipation, smoothing), especially in the case of flows with shocks. The boundary conditions may themselves be a source of error, which may take the form of erroneous vorticity. One attempts to minimize the effect of the artificial viscosity, but it will always represent another mechanism for the generation of vorticity. Viscous-like effects generated by artificial viscosity must be considered numerical error and we must be careful when attaching a physical interpretation to such flows.

Presented as Paper 84-0524 at the AIAA 22nd Aerospace Sciences Meeting, Reno, NV, Jan. 9-12, 1984; received Feb. 10, 1984; revision submitted April 25, 1985.

*Research Scientist, Numerical Aerodynamic Simulation Projects Office.

†Research Scientist, Computational Fluid Dynamics Branch.

This paper will discuss the phenomenon of flow separation for inviscid and viscous flow calculations. The code used for the calculations is an implicit, Beam-Warming approximate factorization of the Euler and thin-layer Navier-Stokes equations. Either of these two sets of equations can be solved, the choice being made by an input parameter. It has evolved from the code written by Steger.[2] For a more detailed description of the code, see the paper by Pulliam et al.[3] or the review article by Pulliam.[4] The code has been used extensively for both viscous calculations[5] and inviscid solutions.[6]

The code is based on an implicit approximate factorization finite difference scheme that can be either first- or second-order accurate in time. The spatial derivatives are approximated by second-order central differences. Explicit fourth-order and implicit second-order smoothing terms are added to enhance the nonlinear stability. When run in the viscous mode, the code employs the thin-layer approximation for the viscous terms in which viscous derivatives in the streamwise direction are neglected, while viscous terms in the normal direction are retained. The turbulence model used is the Baldwin-Lomax model.[7] Details can be found in the above-mentioned papers.

We shall perform studies to assess the effect of artificial viscosity and shock-induced vorticity. The studies will include a case in which separation and self-induced oscillation appear to mimic plausible physical behavior, but is shown to be numerical in origin. In another case, we present evidence that the observed oscillations are indeed solutions to the Euler equations. The final case is one for which experimental data exist. The last case is calculated both inviscidly and with the viscous option of the code. The comparison of these calculations aids in the physical interpretation of the Euler result. The viscous calculation is compared with experiment in order to validate the viscous code.

An algebraic grid generator written by Dennis Jespersen of NASA Ames was used to create the grids used for inviscid calculations in this paper. All the cases presented were run time accurately from freestream initial conditions.

Inviscid Computations

Examples of candidate flows are given by conditions about a NACA 0012 airfoil in a range of Mach numbers of 0.25-0.4 at high angles of attack (13.5-15.0 deg).

Mach 0.4, Coarse Grid

The first example calculated is an inviscid flow with separation and recirculation. The time history for the coefficient of lift is shown in Fig. 1 and demonstrates the periodic nature of the flow. The flow conditions are a Mach number $M_\infty = 0.4$ and angle of attack $\alpha = 15.0$ deg. The computation was run time accurately and, in this case, an unsteady flow is obtained, with a periodic oscillation. The Strouhal number, a nondimensionalized shedding frequency, is defined by

$$S = \omega d / U$$

where ω is the shedding frequency, d the nondimensional length scale, and U the freestream velocity. Figure 1 shows that this case has a periodic and regularly repeating oscillation of 500 iterations. Using the chord length of 1.0 for d, a freestream velocity of 0.4, and a frequency of 1/20 (500 iterations at a time step of 0.04), we get a Strouhal number of 0.125. A Strouhal number of 0.16 for oscillating flow about a cylinder has been computed by Pieter Buning of NASA Ames,[8,9] using a flux-split algorithm for the Euler equations. The experimentally observed Strouhal number is about 0.2 for low Mach number laminar flows about a cylinder.[10] One would not expect the Strouhal numbers to be identical for a cylinder and an airfoil, but it is of interest to note how close they are.

A description of the evolution of this case is described in detail later in this paper. Briefly, the features to be noted are the presence of a strong shock near the leading edge, followed by the formation of a large region of separated, recirculating flow over the midsection of the body. The region of separation is convected off the body and the pattern repeats itself. This flow pattern has a well-defined period and amplitude and has been reproduced in other computations with similar grids and different values of time step and artificial viscosity.

Mach 0.25, Coarse Grid

In order to ascertain the effect of the shock in the generation of separation and consequent self-induced oscillation, cases were run at lower Mach numbers. These calculations were intended to determine what disappeared first as the freestream velocity decreased, the shock or the oscillation. At a Mach number of 0.25, but with all other conditions (code, grid, and all other parameters) the same, a self-induced oscillation was discovered, without the occurrence of any supersonic points in the field at any point during the period. A time history of the lift coefficient is shown in Fig. 2a showing oscillatory behavior. The production of entropy at the leading edge of the airfoil for the previous case at a Mach number of 0.4 is shown in Fig. 2b. Figure 2c has the contours of the entropy at the leading edge for the case of Mach 0.25. The fact that there was no shock at any point during the time history of this case demonstrates that oscillation can occur without shocks.

The entropy creation shown in Fig. 2c is clearly erroneous, for the slip boundary conditions that are imposed on the Euler equations do not provide any mechanism to produce entropy. This differs from the no-slip boundary conditions at the body for the Navier-Stokes equations. In contrast with the previous case, the production of entropy is an error at

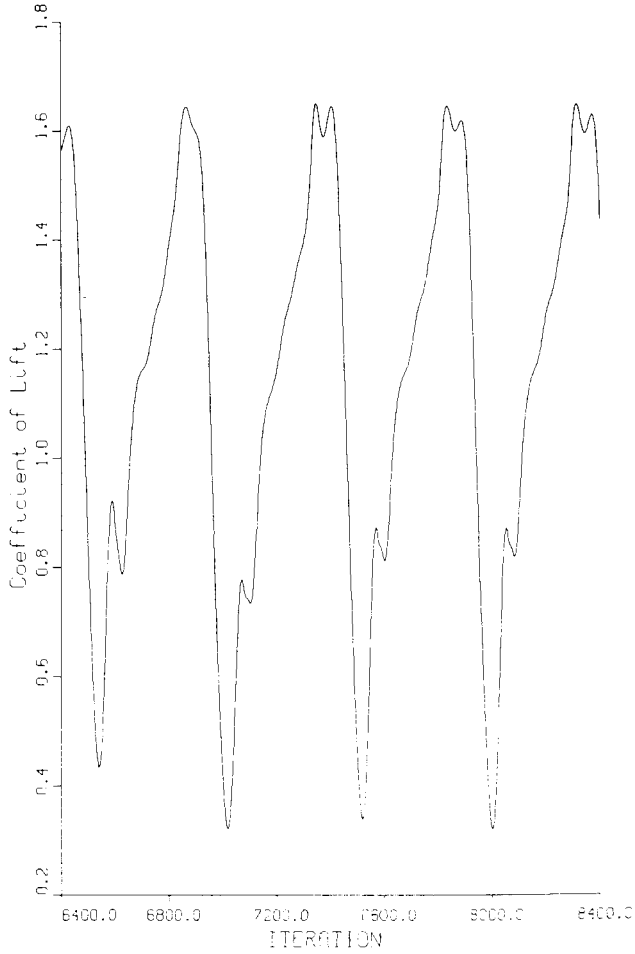

Fig. 1 Lift coefficient history for $M_\infty = 0.4$, $\alpha = 15$ deg, coarse grid.

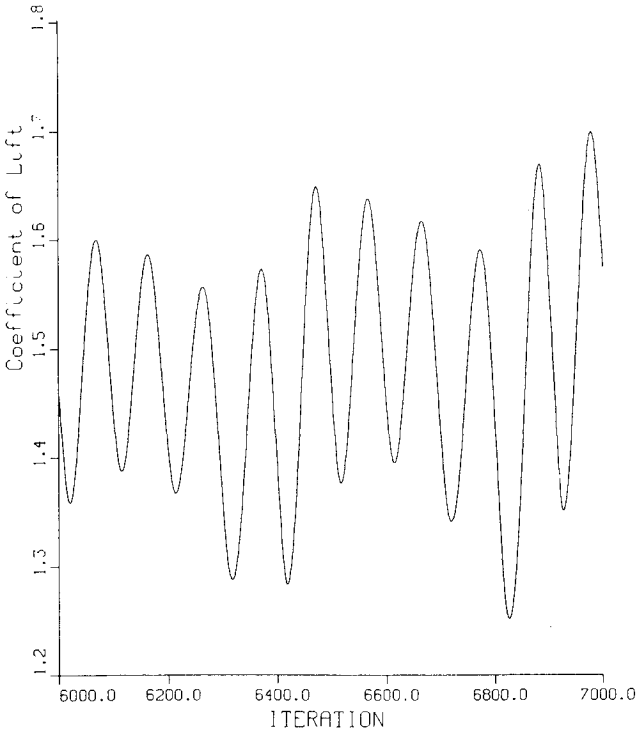

Fig. 2a Lift coefficient history for $M_\infty = 0.25$, $\alpha = 15$ deg, coarse grid.

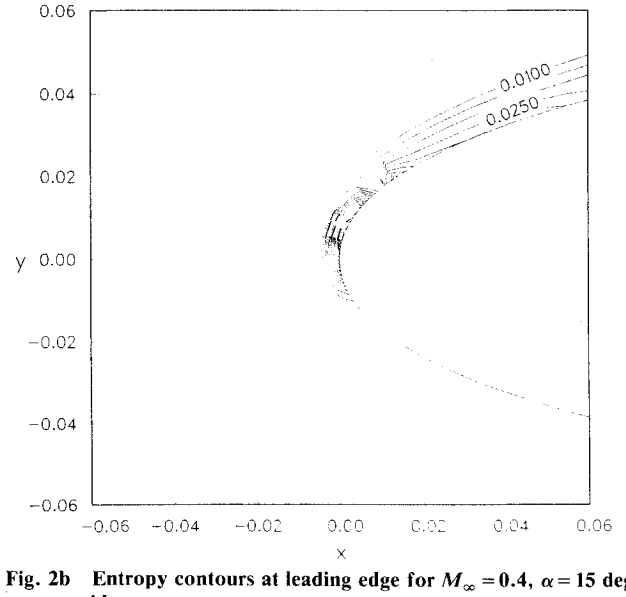

Fig. 2b Entropy contours at leading edge for $M_\infty = 0.4$, $\alpha = 15$ deg, coarse grid.

the leading edge, in the absence of a shock. This different mechanism mimics the effect of a viscous boundary layer. The flow structure appears similar to a separated boundary layer, with subsequent wake oscillation. The period of this oscillation is four times faster than that induced by the larger-scale separation in the previous case at Mach 0.4. This more rapid oscillation can be seen in entropy contour plots where an alternate upward and downward angle is present in the contour lines leaving the trailing edge of the body. In order to test the hypothesis that numerical errors at the leading edge are responsible for this latter separation, two methods were used to reduce that error: the grid was refined in the normal direction and an improved numerical boundary condition at the body was employed. The motivation for grid clustering was that there are large gradients occurring in the normal direction.

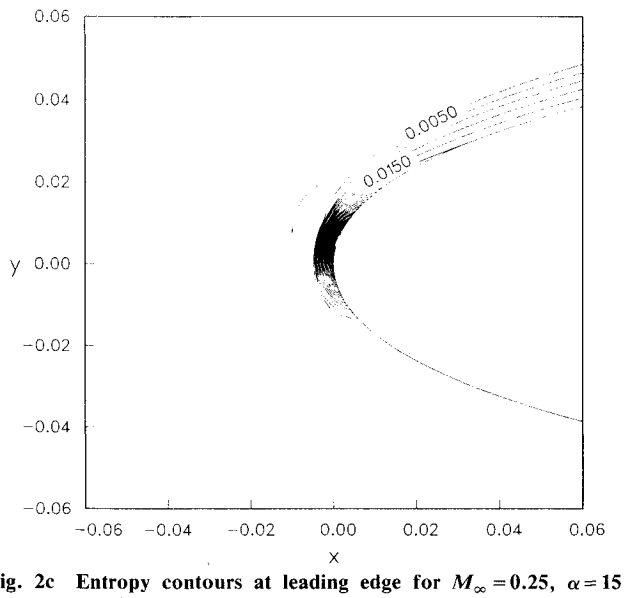

Fig. 2c Entropy contours at leading edge for $M_\infty = 0.25$, $\alpha = 15$ deg, coarse grid.

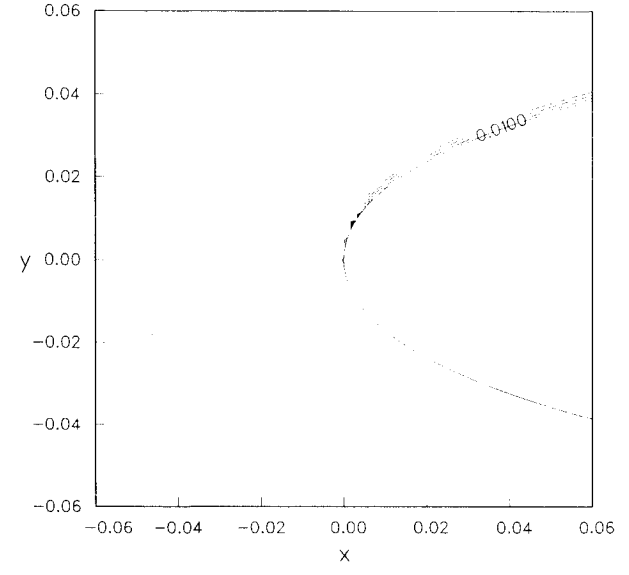

Fig. 3 Entropy contours at leading edge for $M_\infty = 0.25$, $\alpha = 15$ deg, fine grid.

Mach 0.25, Fine Grid

The grid used for the above two calculations has a minimum Δx at the leading edge of 0.002 (based on chord), and 0.004 at the trailing edge. The minimum spacing in the direction normal to the body is 0.005 and the outer boundaries are 12 chord lengths upstream and 24 chord lengths to the sides and downstream. Another grid was generated, with identical disposition of 249 points parallel to the body, 34 in the wake, 90 on the lower surface, and 91 on the upper. No change was made in the grid spacing in the direction of flow next to the body. Normal to the body, however, there are 67 instead of 41 points and a minimum spacing off the body of 0.001, a factor of five finer than before. This refinement in the direction normal to the flow near the body is intended to decrease any numerical errors near the body. The result for the Mach 0.25, 15 deg α case has a shock and no separation. See Fig. 3. The lift coefficient is constant and the calculation converges, rather than behaving periodically. For this case, the shock is much weaker than it was for the previous case at Mach 0.4. It does not provide enough of an entropy gradient to produce unsteadiness or separation.

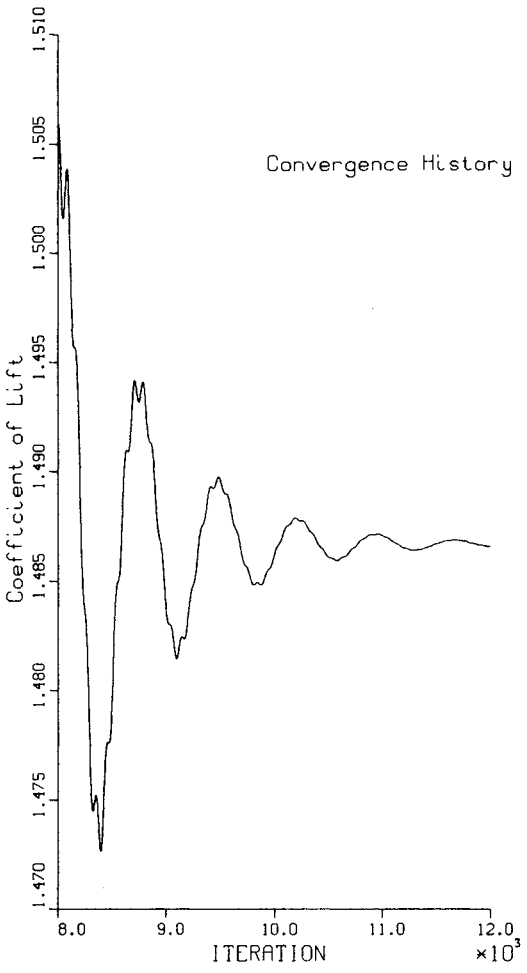

Fig. 4 Lift coefficient history for $M_\infty = 0.25$, $\alpha = 15$ deg, coarse grid, normal entropy boundary conditions.

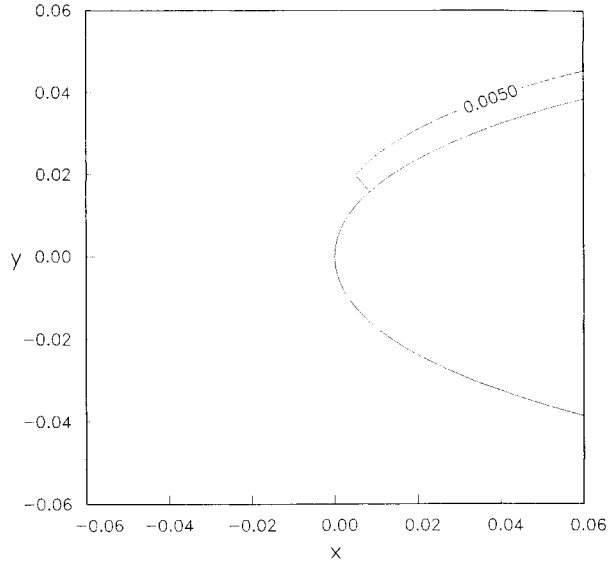

Fig. 5 Entropy contours at leading edge for $M_\infty = 0.25$, $\alpha = 15$ deg, coarse grid, normal entropy boundary conditions.

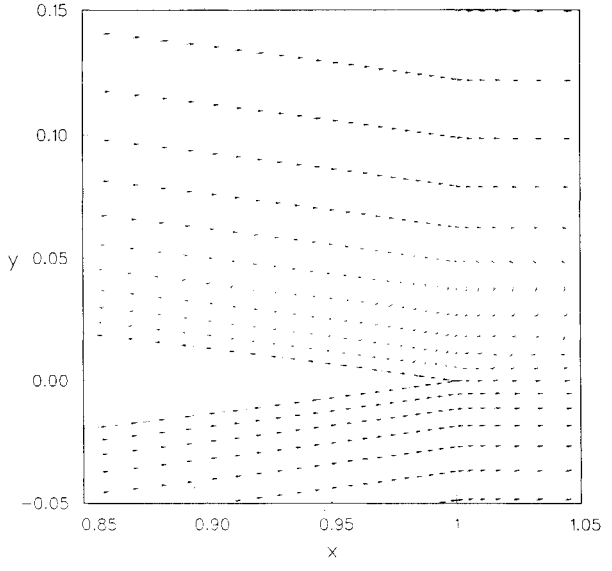

Fig. 6 Velocity vectors showing separation for $M_\infty = 0.25$, $\alpha = 15$ deg, coarse grid.

The reduced mesh spacing has two possible effects on the solution accuracy. It reduces the influence of the artificial viscosity due to the explicit fourth-order and implicit second-order smoothing. It also increases the accuracy of the finite difference approximations, especially in the leading-edge region where high gradients exist due to the rapid expansion around the nose.

Another means of reducing the numerical errors arising from the boundary conditions is to improve them rather than the grid. In order to reduce the entropy errors at the leading edge, the boundary conditions were adjusted to force the normal gradient of the entropy to vanish. This was accomplished by the following procedure. The entropy is calculated from the pressure and density one grid point away from the body. The entropy at the body is fixed at this quantity and one then solves for the density at the body. This amounts to a zero-order extrapolation of the entropy in a direction normal to the body. The choice of this condition was motivated by the buildup of the error at the body itself, rather than in the field. One must be careful not to impose a condition that would not be satisfied at the shock. Since the shocks are all locally normal to the surface for the cases, this boundary condition will not interfere with an entropy jump across any shock. Even when run on the coarser grid with spacing of 0.005 chords normal to the body, the more accurate boundary condition corrected the solution sufficiently to remove the oscillation, and gave a steady, converged solution. The history of the lift coefficient is shown in Fig. 4. The entropy contours plotted in Fig. 5 from the converged solution show the marked reduction in entropy error from those depicted in Fig. 2b. Although steady, the solution still shows separation at the trailing edge, as shown in Fig. 6. The error reduction is not sufficient to remove the erroneous steady separation, which remains even in the absence of any appreciable shock. Although we have reduced the amount of erroneous entropy generation by improving the boundary conditions, a finer grid is still needed to reduce the levels far enough to produce a truly inviscid solution.

To validate the calculation of the steady flow computed on the refined grid, the full potential code TAIR of Holst[11] was used to solve the same flow conditions. The TAIR solution is compared with the solution on the refined mesh (0.001 chords normal to the body). The agreement, which is depicted in Fig. 7, is excellent. A very fine mesh with 149 points on the body was used for the potential calculation.

Mach 0.4, Fine Grid

The self-induced oscillation of the flow at Mach 0.25 seems, therefore, to have been shown to be the product of numerical error. The same techniques to reduce the error in the first case (Mach 0.4) were applied to see if that flow became steady also. First, the boundary conditions were

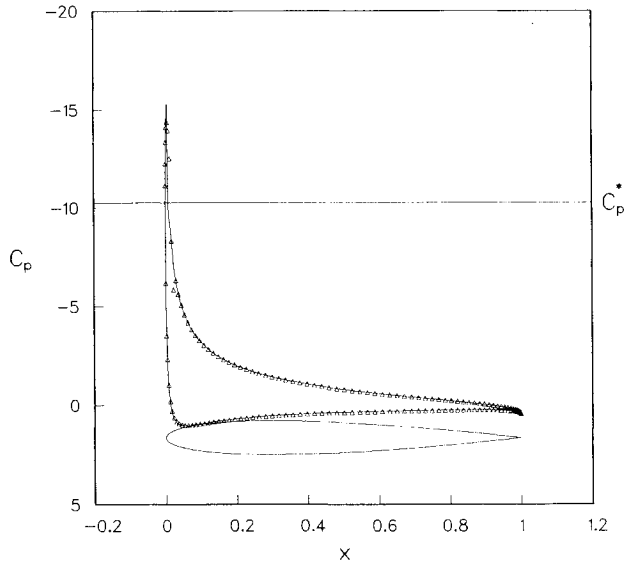

Fig. 7 Pressure coefficient comparison with potential TAIR (Holst) for $M_\infty = 0.25$, $\alpha = 15$ deg, fine grid, normal entropy boundary conditions.

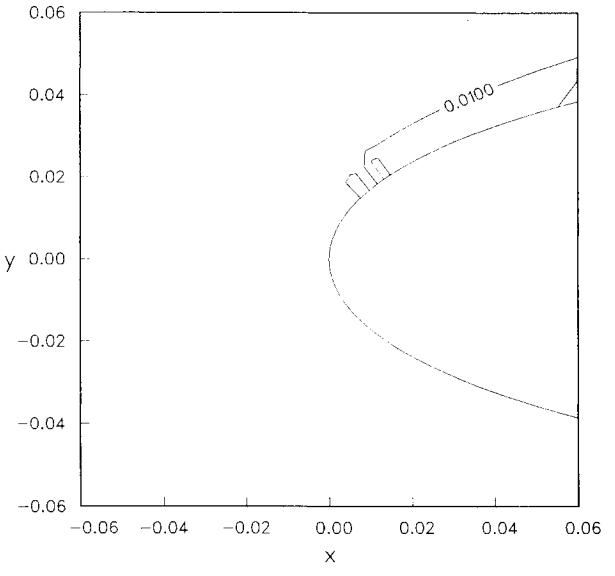

Fig. 8 Entropy contours at leading edge for $M_\infty = 0.4$, $\alpha = 15$ deg, coarse grid, normal entropy boundary conditions.

changed to maintain a vanishing normal gradient of entropy. The flow that resulted was almost indistinguishable from that generated with the original boundary conditions. The plot of entropy contours near the leading edge shown in Fig. 8 clearly demonstrates the effect of the new boundary condition, namely, the reduction in the entropy production at the leading edge.

The final calculation for Mach 0.4 was done on a grid refined to 0.001 of chord in the normal direction. The normal entropy boundary condition was used. Due to the difficult nature of this computation, the time step had to be reduced to 0.005 and the smoothing coefficient was increased by a factor of 1.5. The resulting flow is similar to the calculations at this Mach number on the coarser grid with and without normal entropy boundary conditions, indicating that the resulting separation is not due to numerical error. The history of the coefficient of lift is shown in Fig. 9. The Strouhal number for this calculation is 0.12. The behavior of the coefficient of lift in Figs. 1 and 9 is, of course, not identical, but the fact that the separation is qualitatively the same

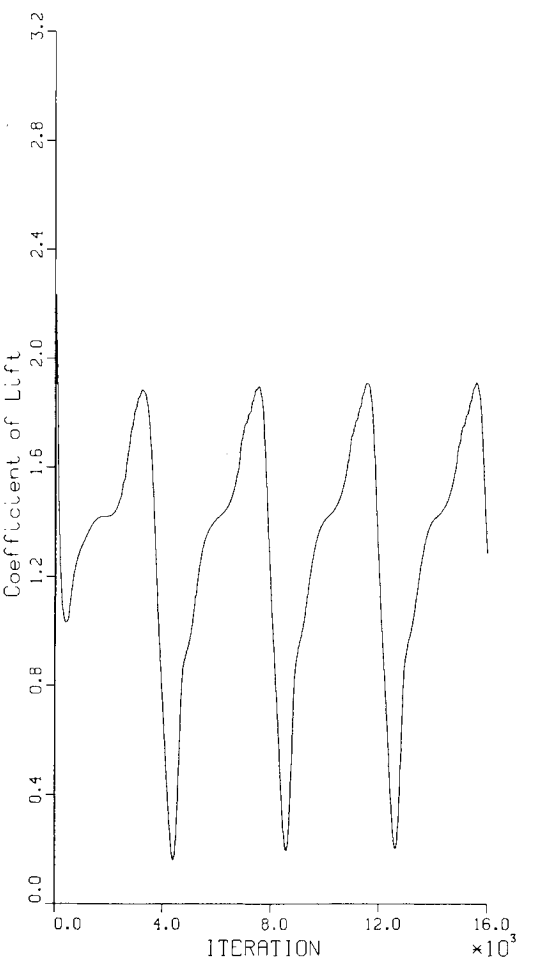

Fig. 9 Lift coefficient history for $M_\infty = 0.4$, $\alpha = 15$ deg, fine grid, normal entropy boundary conditions.

shows that it is not due to numerical errors. The significant feature of either Fig. 1 or 9 is the existence of periodicity in time of the flow features. The periodicity in the two figures is of comparable extent and the general behavior over one period is qualitatively the same in the two cases.

The authors have investigated this time-dependent flow by examining a series of plots of the stream function at a refined series of time steps over one period. A description of the evolution of this case is as follows. As the flow develops, a strong shock is generated at the leading edge. Entropy, vorticity, and pressure loss are created at the shock near the leading edge and convected downstream along the body. A small separation region appears at the trailing edge, which grows along the body toward the leading edge. At some point, the recirculation region is captured by the oncoming flow and is swept off the airfoil by convection. As the recirculation region passes the trailing edge, another pocket of recirculation forms at the trailing edge, rotating in the opposite direction. This counter-rotation is caused by the flow off the lower surface, whose direction is opposite to that of the original region of recirculation. The shock then collapses and begins to slowly grow in strength as the pattern repeats itself. This flow pattern has a well-defined period and amplitude and has been reproduced in other computations with similar grids and different values of time step and artificial viscosity.

The principal difference between the solutions at Mach 0.25 and 0.4 on the fine grid is the strength of the shock present in the Mach 0.4 case. Just as the curved shocks present in the flows over circular cylinders give rise to vorticity, so does the strong but short shock in this case. The strength of this shock is illustrated by the Mach number contour plot

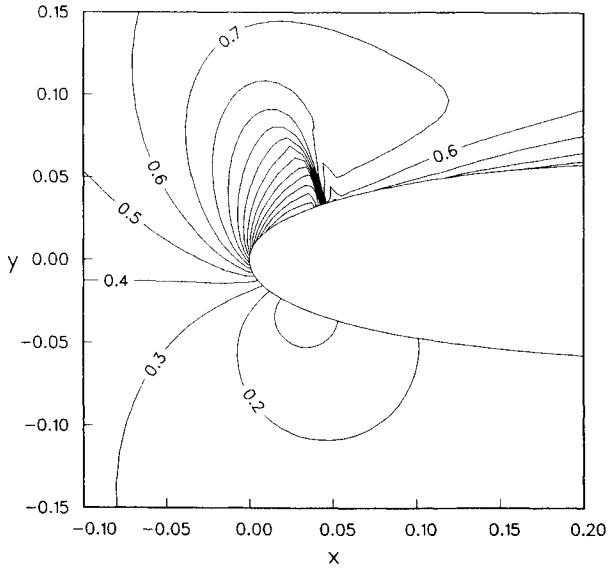

Fig. 10a Mach contours at leading edge showing strong shock for $M_\infty = 0.4$, $\alpha = 15$ deg, fine grid, normal entropy boundary conditions.

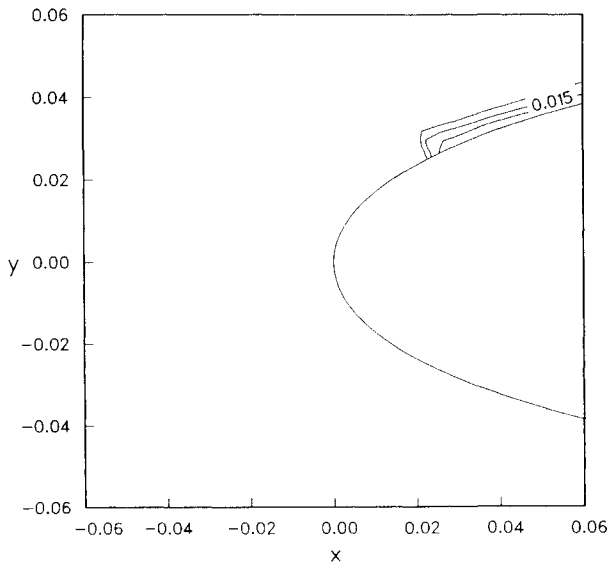

Fig. 10b Entropy contours at leading edge showing error reduction for $M_\infty = 0.4$, $\alpha = 15$ deg, fine grid, normal entropy boundary conditions.

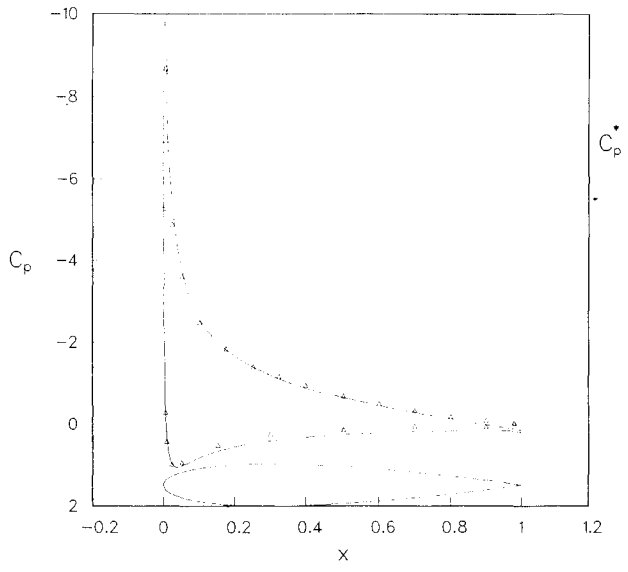

Fig. 11 Pressure coefficient comparisons of thin-layer Navier-Stokes with experimental data of McCroskey for $M_\infty = 0.301$, $\alpha = 13.5$ deg, $Re = 3.91 \times 10^6$.

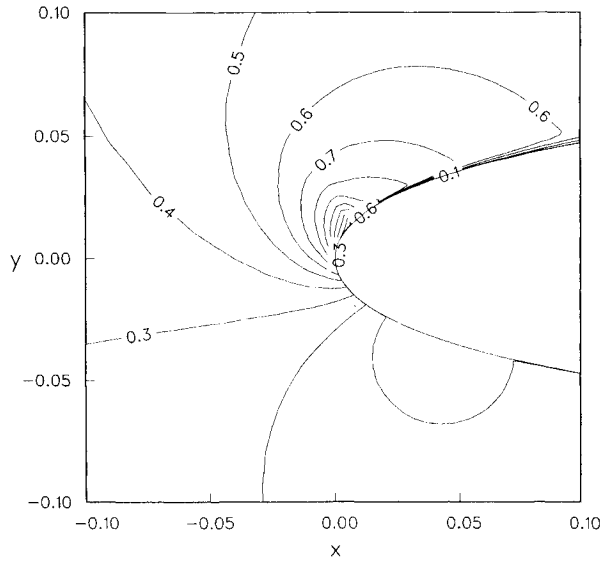

Fig. 12 Mach contours at leading edge for $M_\infty = 0.301$, $\alpha = 13.5$ deg, $Re = 3.91 \times 10^6$, thin-layer Navier-Stokes.

in Fig. 10a. The vorticity produced near the leading edge, in turn, convects downstream and feeds the growing region of recirculation at the trailing edge of the airfoil. This region grows until it breaks off and convects downstream. The reduction of leading-edge entropy errors for the case at Mach 0.4 on the fine grid is shown in Fig. 10b. The normal entropy boundary conditions were used.

Conclusions for Inviscid Cases

We have presented here cases of inviscid flow with seemingly contradictory results. In the Mach 0.4 case, flow separation exists in the presence of a shock at the leading edge. The shock is a source of the vorticity needed to produce separation. By itself, the physical interpretation of this flow seems reasonable. In contrast, we have computed another case, that at Mach 0.25 on a coarse grid, in which flow separation can occur without the existence of the shock. The only other sources of vorticity that might cause this separation are the artificial viscosity and/or numerical error due to mesh coarseness. We have shown that refining either the grid or the boundary conditions can suffice to reduce the errors sufficiently to get a steady solution. The persistence of the same oscillating solution in the Mach 0.4 case, despite such refinements, supports the hypothesis that the self-induced oscillation is inherent in the Euler equations for the given flow conditions. This indicates that it is the entropy production at the shock which is responsible for the separation occurring in the Mach 0.4 case.

Viscous Computations

Viscous solutions were also obtained using the thin-layer Navier-Stokes equations. These computations have a twofold purpose: they validate the computation by comparison with experiment and they are intended as control cases to compare against the inviscid computation. The flow conditions were a Mach number $M_\infty = 0.301$ and $\alpha = 13.5$ deg. The Reynolds number $Re = 3.91 \times 10^6$ and the calculation was

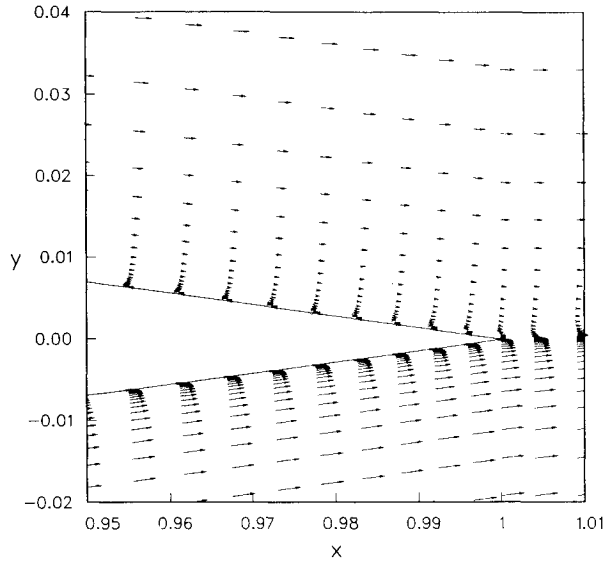

Fig. 13 Velocity vectors at trailing edge showing limited extent of separation for $M_\infty = 0.301$, $\alpha = 13.5$ deg, $Re = 3.91 \times 10^6$, thin-layer Navier-Stokes.

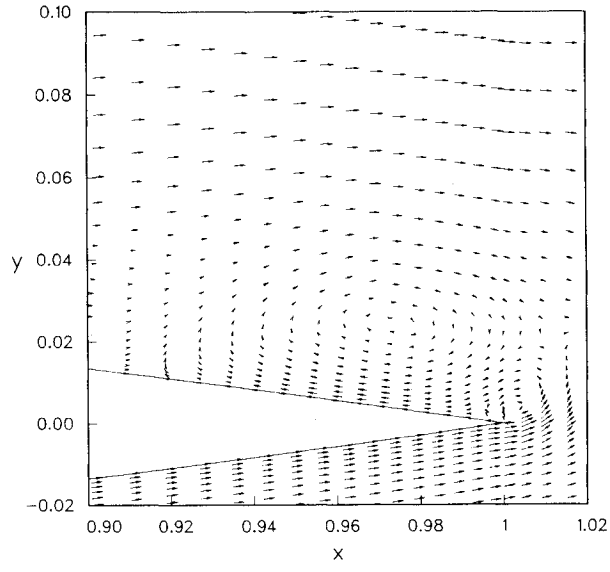

Fig. 15 Velocity vectors at trailing edge showing greater extent of separation for $M_\infty = 0.301$, $\alpha = 13.5$ deg, Euler solution, fine grid.

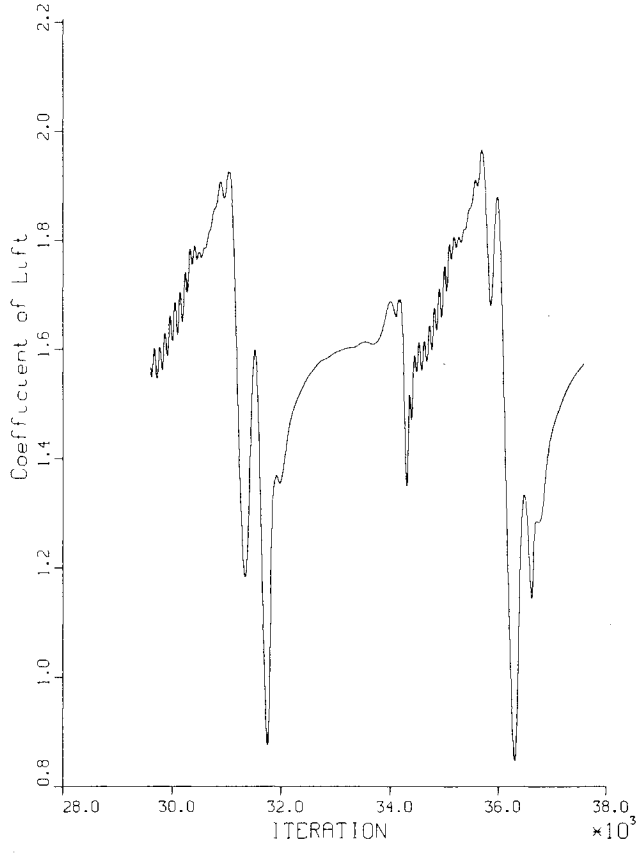

Fig. 14 Lift coefficient history for $M_\infty = 0.301$, $\alpha = 13.5$ deg, Euler solution, fine grid, normal entropy boundary conditions.

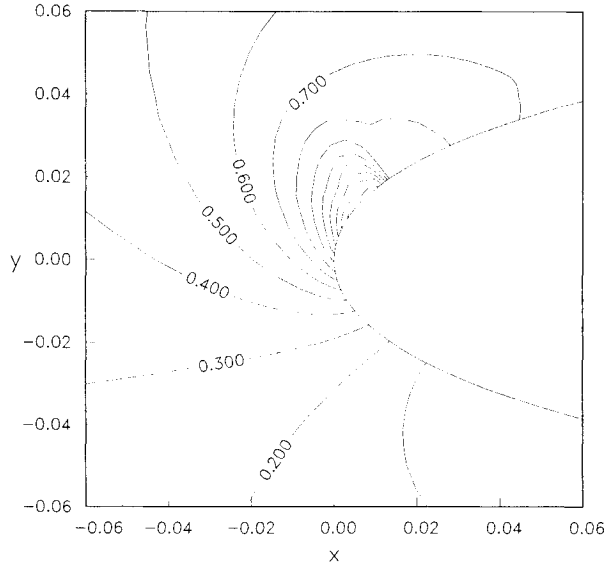

Fig. 16 Mach contours at leading edge showing strength of shock for $M_\infty = 0.301$, $\alpha = 13.5$ deg, Euler solution, fine grid.

performed using an algebraic eddy-viscosity turbulence model.

An algebraic grid was used for the viscous calculation. It had 249×51 points, with 35 in the wake. The outer boundary was 24 chord lengths in front and 48 chord lengths on the sides and in back. The spacing along the body was 0.002 of chord at the nose and 0.004 at the tail. The normal spacing was 0.00002 of chord.

Experimental data available from McCroskey et al.[12] for this case is used for comparison. Figure 11 shows the pressure coefficient for the calculation and the experiment. The calculation yielded a steady converged solution. We interpret the extremely good agreement as affirming the accuracy of the code and the value of the thin-layer Navier-Stokes approximation. The Mach contours in Fig. 12 show a small supersonic bubble at the leading edge. There is also a small region of reversed flow at the trailing edge as depicted by the velocity vectors in Fig. 13. Note that the region of separated flow is restricted to a thin layer and does not extend into the main field, as it had in the inviscid calculations.

Inviscid Comparison

Since the inviscid separation seen in the calculation at Mach 0.4 was qualitatively quite different than the viscous separated solution at Mach 0.301, the inviscid solution for this case (Mach 0.301, 13.5 deg angle of attack) was calculated on the fine grid used for the other inviscid calculations. The normal entropy boundary conditions were used. The same sort of self-induced oscillation seen for the case at Mach 0.4 was reproduced at the somewhat lower Strouhal number of 0.074. The history of the lift coefficient is shown in Fig. 14 for the fine inviscid grid using the normal entropy

boundary conditions. Figure 15 shows the separation at the trailing edge at one point in time for the inviscid calculation. It has considerably greater extent than the separation bubble on the viscous case, but is smaller than in the Mach 0.4 case. The Mach contours at the leading edge in Fig. 16 demonstrate the presence of a shock. The maximum Mach number before the shock is 1.4 for this case, as compared with 1.8 for the Mach 0.4 case. The weaker shock is the reason for a smaller separation region.

Assuming the validity of the inviscid oscillation for this case, we conclude that the Euler solution is not a good approximation to the Navier-Stokes solution, under these conditions. It should be noted that other factors we have not yet considered may be influencing the discrepancy between the viscous and inviscid solutions. The turbulence model, an algebraic eddy-viscosity model, is certainly having some effect on the viscous solution. The choice of point of transition from laminar to turbulent flow on the body may also effect the outcome of the calculation. This raises the important question of determining useful guidelines for deciding when computed quantities from an Euler calculation should be considered representative of what a viscous calculation would give at the same conditions.

Conclusion

Our calculations show that separation in Euler calculations can occur, and may have different interpretations. In the case of the lower Mach number (0.25) at 15 deg angle of attack, the separation was traced to numerical error. In particular, the erroneous entropy generation at the leading edge was the main source of error and it could be reduced by improving boundary conditions and refining the mesh in the normal direction at the body. In the higher Mach number case (0.4) at 15 deg angle of attack, the self-induced oscillation was attributed to vorticity produced at the strong but short shock that formed on the highly curved region of the airfoil just past the leading edge. This conclusion is based on the insensitivity of that solution to reduction in the errors just discussed.

There is excellent agreement between a viscous calculation and experimental data. The same conditions of Mach 0.301 and 13.5 deg angle of attack, when run inviscidly, give results like the self-induced oscillation seen in the Mach 0.4 case. We conclude that an Euler solution may correctly show separated flow that differs considerably from the separation that would occur in a viscous calculation.

References

[1]Salas, M. D., "Recent Developments in Transonic Euler Flow over a Circular Cylinder," *Mathematics and Computers in Simulation*, Vol. XXV, 1983, pp. 232-236.

[2]Steger, J. L., "Implicit Finite-Difference Simulation of Flow about Arbitrary Two-Dimensional Geometries," *Journal of Computational Physics*, Vol 16, 1978, pp. 679-686.

[3]Pulliam, T. H., Jespersen, D. C., and Childs, R. E., "An Enhanced Version of an Implicit Code for the Euler Equations," AIAA Paper 83-0344, Jan. 1983.

[4]Habashi, W. G., Editor, *Advances in Computational Transonics*, Pineridge Press, Ltd., Swansea, U.K., 1983.

[5]Steger, J. L. and Bailey, H. E., "Calculation of Transonic Aileron Buzz," *AIAA Journal*, Vol. 18, March 1980, pp. 249-255.

[6]Pulliam, T. H. and Barton, J. T., "Two Dimensional Euler Solutions for AGARD Test Cases," NASA TM, to be published.

[7]Baldwin, B. S. and Lomax, H., "Thin Layer Approximation and Algebraic Model for Separated Turbulent Flows," AIAA Paper 78-257, Jan. 1978.

[8]Buning, P. G., "Computational of Inviscid Transonic Flow Using Flux Vector Splitting in Generalized Coordinates," Ph.D. Thesis, Stanford University, Stanford, CA, 1983.

[9]Buning, P. G. and Steger, J. L., "Solution of the Two-Dimensional Euler Equations with Generalized Coordinate Transformation Using Flux Vector Splitting," AIAA Paper 82-0971, June 1982.

[10]Roshko, A., "Experiments on the Flow Past a Circular Cylinder at Very High Reynolds Number," *Journal of Fluid Mechanics*, Vol. 19, Pt. 3, 1961, p. 345.

[11]Holst, T. L., "Implicit Algorithm for the Conservative Transonic Full-Potential Equation Using an Arbitrary Mesh," *AIAA Journal*, Vol. 17, Oct. 1979, pp. 1038-1045.

[12]McCroskey, W., McAlister, K., Carr, L., and Pucci, S., "An Experimental Study of Dynamic Stall on Advanced Airfoil Sections, Vol. 1: Summary of Experiment," NASA TM 84245, 1982.